THE JOURNAL OF PHYSICAL CHEMISTRY B

Article

pubs.acs.org/JPCB

Phase Transitions of *n*-Hexadecane in Nanoencapsulated Binary Solutions of *n*-Hexadecane and 1-Octanol

Kyle W. Tubbs, Vincent T. Nguyen, and Thorsteinn Adalsteinsson*

Department of Chemistry & Biochemistry, Santa Clara University, Santa Clara, California 95053, United States

Supporting Information

ABSTRACT: Binary solutions of *n*-hexadecane and 1-octanol were encapsulated within poly(*tert*-butyl methacrylate) nanocapsules and the phase transition behavior of the *n*-hexadecane studied. A sigmoidal correlation was found between the binary composition of the encapsulated oil and the oil formulation prior to encapsulation. At low 1-octanol fractions in the synthesis, almost no alcohol was encapsulated, but at high 1-octanol fractions, the capsules were enriched in alcohol. The freezing point of the encapsulated *n*-hexadecane was considerably lower than in the bulk phase. This freezing point was further reduced as the radius of the particle was reduced, which is expected from the Gibbs−Thompson equation. The extracted value at infinite radii was, however, 14 °C below the bulk freezing point. The colligative effect of 1-octanol on the freezing point of *n*-hexadecane, i.e., dT_f/dx_m, where x_m is the mass fraction of 1-octanol, was nearly identical to that measured in the bulk system. The specific enthalpy of freezing for the encapsulated system was considerably different from the bulk system. In the bulk system, the freezing enthalpy for *n*-hexadecane was nearly constant up to 60% mass of 1-octanol. The freezing enthalpy for the encapsulated *n*-hexadecane showed greater variation with % mass 1-octanol, and had a considerably lower absolute value than the bulk system.

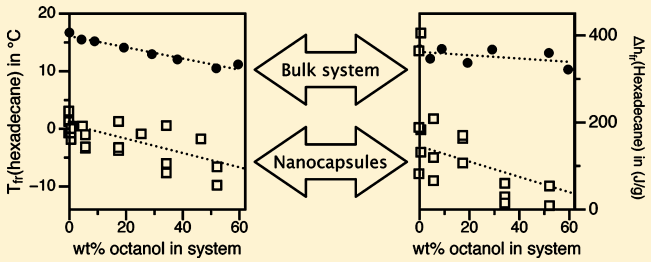

INTRODUCTION

Oil-filled nanocapsules derived from mini-emulsion templates[1−8] are a class of colloids that receive attention for their application potential as well as being important for fundamental science. The advantages of encapsulating ultrasmall, monodisperse droplets of oil solutions within nanometer-thick polymer shells should be fairly obvious, especially if the shell can be removed at a later point. Such particles may function as nanoreactors, nanoprinting vesicles, and carriers for drugs, nutrients, and catalysts to name a few possibilities. There are significant obstacles to going from a core−shell particle architecture to an actual application.[9] One such obstacle is that the polymer shell has unique physical properties from the bulk polymer.[10−12] For thin (flat) polymer films, the underlying substrate greatly affects the glass transition temperature and wetting behavior of the film. Another obstacle is that a large fraction of the encapsulated molecules are physically close to an interface, and therefore behave as thin films rather than a bulk system. Thin (flat) oil films have very different kinetic behavior, i.e., viscosity, than the bulk system does, due to the packing of the oil molecules in the film.[13] The dynamic behavior may be observed in thermal behaviors, such as wetting, miscibility, and phase transitions. This unique behavior can be expected to translate as well to liquids that are confined in other ways. Not knowing how miscibility works in confined volumes is a deterrent to integration of such nanostructures as functional components. Unique phase transitions and thermal behavior have been demonstrated and simulated for water in confined geometries.[14−16] Our basic understanding of oil nanovolumes comes primarily from emulsion systems that do not provide rigid confinement geometries.[17−23] The behavior of oils in emulsion droplets is greatly influenced by the kinetics and packing of molecules at the oil/surfactant interface[23−25] which is governed by the dynamics and packing of the surfactant molecules. Fewer studies have been done on oils in polymers or other solid confinements,[26] where surfactant governed behavior is absent.

The thermal behavior of *n*-alkanes and binary solutions of *n*-alkanes has received much attention, since these systems are immensely important in industry.[27−29] Many of the thermal behaviors of these systems appear to carry over to microvolumes. As an example, transitions from the liquid phase to the rotator phase are observed in microencapslations, although this transition appears at different temperatures.[25] Geometric confinement causes a significant lowering of the freezing point of oils, but the melting point is only slightly lowered. It is still unclear if this effect is due to lack of nucleation sites, to a kinetic arrest of the phase transition,[18,21,30] or to thermodynamic effects such as surface tension, molecular packing, or surface crystallization at the curved solid/liquid interface.[24,31]

The primary objective in this work is to collect experimental evidence for phase transition of pure and binary oil solutions in nanovolumes. We have previously studied encapsulated *n*-hexadecane droplets in polystyrene capsules[32] and in a family of alkyl-methacrylate polymer capsules.[33] This paper

Received: November 28, 2011
Revised: March 2, 2012
Published: March 5, 2012

presents results from studies of binary mixtures of 1-octanol and *n*-hexadecane, which are completely miscible but show single phase transitions (no rotator phase) at two very different temperatures.

MATERIALS AND METHODS

All chemicals were purchased from Sigma-Aldrich in the highest available purity. *tert*-Butyl methacrylate (tBMA) was vacuum distilled twice to remove free-radical scavengers. The initiator, 2,2′-azobisisobutyronitrile (AIBN), was used as received. Sodium dodecyl sulfate (SDS) was recrystallized from 2-propanol to remove impurities and stored under nitrogen. Ultrapurified water with resistivity in excess of 10 MΩ was used as the aqueous phase. 1-Octanol (OCT) and *n*-hexadecane (HD) were used as received.

Instrumental Methods. Particle sizes were determined using a Brookhaven Inc. 90 Plus dynamic light scattering (DLS) instrument equipped with an avalanche photodiode detector. Particle sizes (intensity average) were determined for highly diluted particle suspensions in prefiltered, 5 mM KCl solutions. Solutions with excess surfactant showed multimodal particle size distributions with one population in the 5 nm range and one in the typical particle size range (200 nm).

NMR experiments were done on a 400 MHz Bruker Avance III spectrometer. Quantitative NMR spectra and variable temperature experiments were performed using a Bruker HR-PABBO direct detection probe. Pulsed field gradient NMR spectroscopy, PFG-NMR, using a microimaging Bruker DIFF-30 probe were performed to validate the DLS experiments on select samples.

Differential scanning calorimetry, DSC, experiments were performed on a Mettler-Toledo DSC 823^e calorimeter outfitted with a 24 point FRS-5 thermocouple array. Typical measurements were performed on 20−30 μL of liquid sample in a 40 μL pierced-lid aluminum crucible.

Viscometry was done using Ostwald viscometers placed in a constant temperature bath at 20 °C. The viscometer was calibrated against the viscosity of pure HD and pure water.

Scanning transmission electron microscopy (STEM) images were collected on a Hitachi S-4800 field emission scanning electron microscope at the Santa Clara University Center for Nanostructures (SCU-CNS). High-resolution transmission electron microscope images were collected on a Hitachi H9500 TEM instrument at the UCSC-MACS Facility at NASA-Ames. Samples were collected on Formvar coated 200 mesh copper TEM grids. Particle adhesion to the Formvar film was enhanced by immersing the coated grid in a dilute solution of poly(diallyldimethylammonium chloride) (PDADMAC) in order to give the surface a positive charge. The grid was then allowed to air-dry in a dust-free environment prior to use. Particles were deposited onto the PDADMAC coated Formvar grid by placing a drop of solution on the grid, and wicking excess solution off after 10 min.

Encapsulation of Binary Solutions. We have reported the synthesis method for the capsules elsewhere.[32,33] Briefly, the synthesis is based on formulating a miniemulsion system that contains the monomer, initiator, and all the components that are to be encapsulated as first reported by Tiarks et al.[1] Polymer capsules are obtained when (1) the polymer that is synthesized is insoluble in both the oil phase and in the continuous phase in the emulsion and (2) the polymer has a lower surface tension against the water than the oil does.[34] This is the case when vinyl-type polymers, such as polyamides,[2] polystyrene,[3] and polymethacrylates,[33] are synthesized in particles containing normal alkanes.

In the syntheses here, we used premixed OCT and HD in the desired mass ratios. A 3.5×10^{-3} M SDS solution (approximately 5 times the critical micelle concentration (CMC)) was used as the aqueous phase. Solutions were stored under argon. For a typical synthesis, 1.800 mL of the oil component was mixed with 0.500 mL of the monomer and 1% mole fraction of initiator. This was combined with 15.0 mL of the aqueous phase. The dispersion was then stirred for approximately 20 min under argon flow in a room temperature water bath. Mini-emulsions were prepared by immersing a 3 mm diameter sonicator horn (Misonix XL cell disruptor; operating at 41 kHz at half-maximum power) into the solution, leaving approximately 5 mm space between the bottom of the vial and the horn. The sonicator was turned on for a maximum of 90 s in order to avoid excessive heating of the solution. Multiple sonications were used to further reduce the particle sizes. The polymerization was started by placing the dispersion into an 80 °C bath with mild stirring in order to dissipate heat in the polymerization. The synthesis ran for at least 2 h but no longer than 4 h.

Particles were purified by centrifugation and collected as the top layer of the solution. Samples containing 20% oil to monomer could not be centrifuged due to the matching density of the water and the specific volume of the particles. The flocculent material was redispersed in a 0.5 CMC SDS solution in order to avoid aggregation due to removal of SDS from the polymer particles. A minimum of three purification steps were done to remove unreacted monomers and free micelles from the dispersion.

Quantitative NMR Measurements of Bulk and Encapsulated Oils. Potassium hydrogen phthalate (KHP) was used as a primary standard in order to obtain the mass of components in the NMR sample. A 1D-NMR spectrum of a sample containing 40% OCT (by mass in synthetic formulation) is shown in Figure 1. In order to simplify phasing and baseline correction for the samples, the water signal was suppressed using presaturation pulses without using magnetic field gradients (zgcppr). This solvent suppression had a negligible effect on the NMR signals used in the analysis.

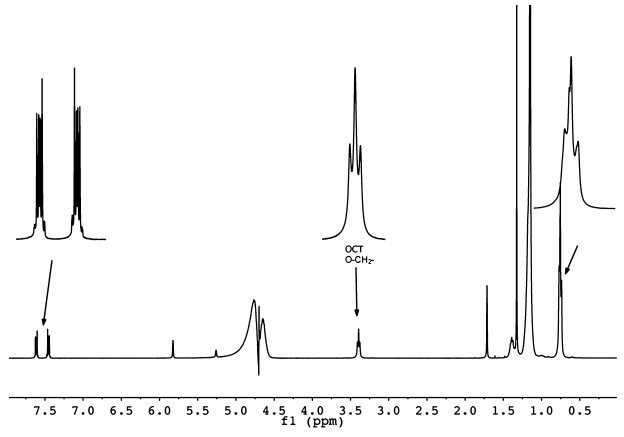

Figure 1. Sample 1D NMR spectrum used for quantitative analysis. The spectrum was collected using the Bruker zgcppr water presaturation pulse program. The peaks from the hydrogen phthalate anion are visible in the region of 7 ppm. The peak at 3.78 ppm is from the O−CH_2 group in OCT. The series of peaks around 0.78 ppm originates from methylene groups in both HD and OCT. From knowing the exact concentration of the KHP, the concentration of both OCT and HD can be calculated.

The area under the aromatic peaks from the KHP corresponds to the four phthalate protons. The area under the

dx.doi.org/10.1021/jp211459j | J. Phys. Chem. B 2012, 116, 3954−3960

multiple peak at 3.75 ppm corresponds to two protons on the O−CH_2 group in OCT. The total area under the broad peak at 0.78 ppm comes from the CH_3 groups on both HD (6H) and OCT (3H). This allows us to calculate the mass fractions for the oils, since the methyl protons should have similar relaxation times.

DSC Measurements. *Bulk Oil Solutions.* Samples for this study were premixed by weight. A 20 μL sample was then weighed into a DSC pan. DSC thermograms were collected between +50 and −50 °C using heating/cooling rates (dT/dt) varied between 20 and 1 °C/min. Typical data of this type is shown in Figure 2. The onset temperatures for each component

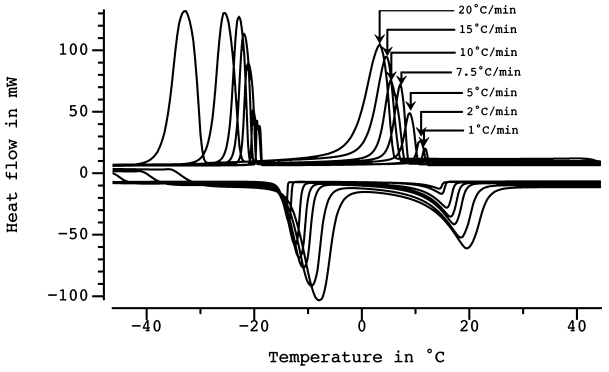

Figure 2. Sample DSC thermograms for 60% mass OCT at various heating and cooling rates. Freezing transitions register as positive peaks in the thermogram. The onset temperature is the intercept between a tangent drawn through the inflection point of the peak and the baseline. The transitions shift with the heating rates, as is indicated in the figure.

in the solution vary with dT/dt due to thermal conductivity and rate of nucleation. According to Taggart et al.,[28] the phase transition temperature is found from linear extrapolation of log(mszw) versus log(dT/dt) in the limit of $dT/dt = 0$, where mszw is the metastable zone width, or the measured difference between the freezing and melting point of the oil component. The area under a peak in the thermogram corresponds to the product of dT/dt and the transition enthalpy, since we use DSC pans at constant pressure. The experimental error of ΔH is therefore higher at low dT/dt. Here we report enthalpy values at heating and cooling rates of 2.5 °C/min.

Encapsulated Solutions. Samples were prepared by combining purified capsule dispersions with 100 mM NaCl solution in order to depress the freezing point of water. The freezing of water significantly affects the subsequent thermal scans of the capsules; viz., the oil shows thermal behavior identical to the bulk system. We have previously discussed that this change is probably due to crushing of the capsules in the ice-crystal.[32] In samples where the water remains unfrozen, we can repeat the DSC scans. DLS experiments show that 50 mM NaCl is sufficient to cause some aggregation of the capsules. We did not notice a systematic change in the phase transition temperature or enthalpy values with salt concentration, even when samples had higher salt concentration than 50 mM. Each DSC run consisted of trials with dT/dt from 2.5 to 1 °C/min over a temperature range from −12 to 30 °C. The freezing point of the encapsulated OCT is well below this value, and we are therefore unable to report this value.

The enthalpy of freezing was calculated from runs using a 2.5 °C/min cooling rate, as in the bulk. The mass of HD in DSC samples was calculated from quantitative NMR measurements of the stock solution. The calculated total mass of HD in the DSC experiments ranged from 0.04 to 0.6 mg.

RESULTS AND DISCUSSION

Particle Morphology and Success of Encapsulation. Figures 3 and 4 show examples of SEM and STEM images of

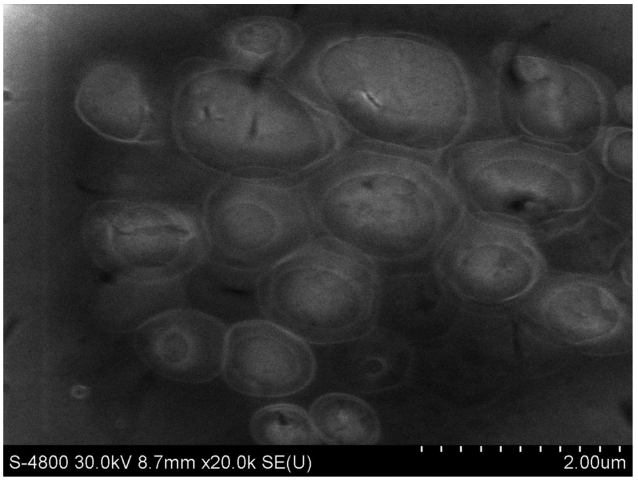

Figure 3. Scanning electron microscopy image of dried poly(*tert*-butyl methacrylate) capsules.

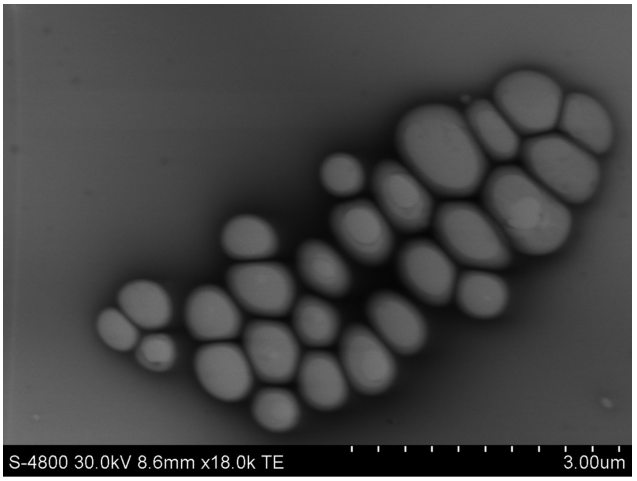

Figure 4. Scanning transmission electron microscopy image of dried poly(*tert*-butyl methacrylate) capsules.

particles. The particles in Figure 3 contained 85 vol % HD and 15 vol % tBMA prior to polymerization. Figure 4 is an STEM image of capsules made with 90 vol % HD and 10 vol % tBMA prior to synthesis. The STEM image is deliberately adjusted to overfocus in order to emphasize the contrast between the Formvar and the polymer film.

Due to the high vacuum environment within the microscope, the capsules were completely dried of all oils, and therefore appeared as flattened particles with a size quite different than the particle radius measured using DLS. The diameters of the particles in the microscopy images were roughly what we would expect if the capsule were flattened into a 30 nm thick disk with the same volume as the original particles. Encapsulation was considered successful if images showed flattened intact bags in the SEM image and dark-haloed vesicle footprints in the STEM

dx.doi.org/10.1021/jp211459j | J. Phys. Chem. B 2012, 116, 3954−3960

image. Incomplete encapsulation showed fragments, no particles, or small polymer particles. The capsules appear to have a rough surface morphology in the SEM image.

Control of Particle Size and Oil Droplet Volume. The hydrodynamic diameter of the particles varied with the time of the sonication and the total viscosity of the oil phase that was being sonicated. Different sonication times gave particle diameters ranging from 250 nm down to approximately 150 nm; see Figure 5. Sonication times of less than 90 s showed a broader

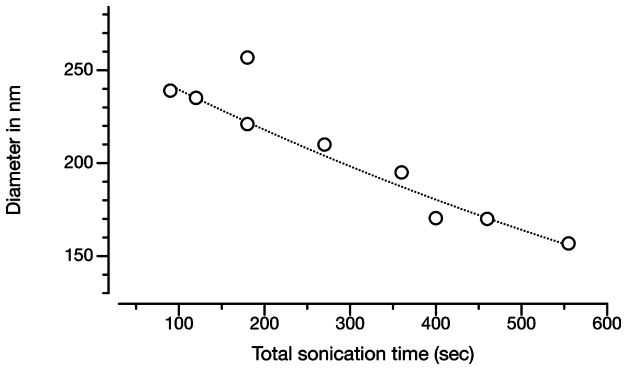

Figure 5. Variation of particle diameters (DLS) as a function of sonication time for particles containing pure HD. The system was sonicated in 30 s increments allowing 90 s between sonications.

distribution of particle sizes, or polydispersity index (PDI). After 90 s, the PDI stabilized to approximately 1.06. Other parameters had little ±10 nm effect on size after 90 s of sonication. This includes the concentration of SDS in the continuous phase (volume of the oil phase constant), although the emulsion was no longer metastable at very low SDS concentrations (particle size changed over 1 h). The ratio of oil to water, either while keeping the SDS to water ratio constant or the SDS to oil ratio constant, did not greatly affect the particle size either.

The composition of the oil phase, which consisted of tBMA, HD, and OCT, clearly affected the particle size. When the OCT to HD ratio increased (fraction of tBMA kept constant), the particle size got considerably smaller. Since changes in the SDS concentration, and thus the oil/water surface tension, did not affect the particle size, we suspect that this effect is a result of the change in viscosity of the oil phase. Figure 6 shows

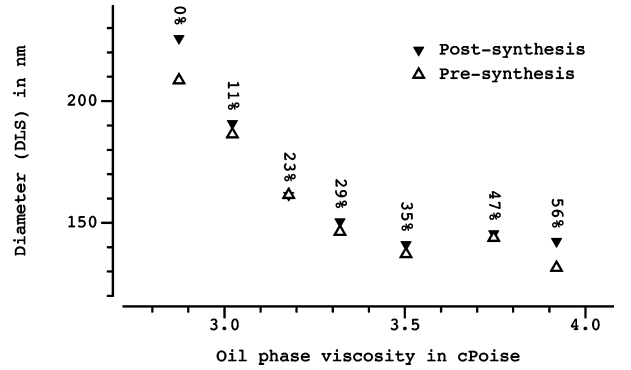

Figure 6. Variation of particle size as a function of measured viscosity of the oil phase. The oil phase in question contained OCT/HD in binary ratios as indicated in the figure. In addition to the oil, the samples contained tBMA and AIBN. The volume ratio of tBMA and OCT+HD was kept constant at 10%. Open triangles show measured particle size prior to synthesis, whereas the closed triangles show post synthesis diameter.

the particle diameter as a function of the measured viscosity of the oil component prior to synthesis. The particle size was measured directly following the sonication, and post purification of the polymer capsules.

The particle radius and the volume fraction of monomer to nonreactive oil (HD and OCT) allow us to estimate the radius of the encapsulated oil droplet according to

$$R_{\mathrm{oil}} = \sqrt[3]{x_{\mathrm{v,oil}}}\,R_{\mathrm{H}} \tag{1}$$

where $x_{\mathrm{v,oil}}$ is the volume fraction of the nonreactive oil to monomer and R_{H} is the hydrodynamic radius according to DLS. Here we assume that the oil is completely enclosed within the polymer shell and that the density of the monomer is identical to the density of the polymer. This assumption is not strictly true—one would expect the polymer to have a slightly higher density than the monomer. Figure 6 shows that the postsynthesis particles were slightly larger than the presynthesis emulsion particles, although this effect may be within the experimental error of the DLS experiment. So far, we have not been able to achieve sufficiently accurate measurements of the particle density pre- and post-synthesis, although such experiments should be possible through analytical centrifugation, or thermogravimetric analysis.

Yield of *n*-Hexadecane/1-Octanol Solutions in Encapsulation. Seven shows the mass fraction of OCT measured by NMR as a function of the mass fraction used in the capsule synthesis from two independent experimental trials. The figure shows that lower mass fractions of OCT in the synthetic solution (OCT < 40%) yielded a smaller than expected fraction in the capsule, while the higher mass percentages (>70%) yielded a higher than expected fraction in the capsule.

The fit through the points follows the form

$$f(x) = \frac{Ax^n}{B + x^n} \tag{2}$$

where x is the mass fraction in the synthesis. The fit line gave values $n = 2.59$, $A = 126 \pm 2$, and $B = 0.25 \pm 0.01$. The exact reason for the sigmoidal shape is not clear to us at this point, but it is worth noting that the shape of the fitted curve resembles a binding isotherm for cooperative binding. (Here we assume that the binding isotherm is described by the Hill equation, $\nu(s, \tau) = \partial \ln[Z(s, \tau)]/\partial \ln[s]$, with $s = K{\cdot}C(A)$, where K is the equilibrium coefficient and $C(A)$ is the concentration of the molecule that is binding to the substrate.) A calculated binding curve with four sites in a tetrahedral geometry (here we use $Z(s, \tau) = 1 + 4s + 6\tau s^2 + 4\tau^3 s^3 + \tau^6 s^4$) can be fitted very closely with eq 2 using $n = 2.59$ and the proper choice of the equilibrium coefficient K for binding and the affinity advantage τ. A calculated binding curve with two or three binding sites does not provide satisfactory agreement with the fitted curve.

Effect of Particle Size on the Phase Transition Temperature of Encapsulated HD. Turnbull,[17,18] and later Charoenrein,[35] proposed that in microencapsulated volumes the nucleation from liquid to the solid phase must occur from a spontaneous fluctuation in the volume (homogeneous nucleation), rather than from a seed particle. Seed particle nucleation, or heterogeneous nucleation, is the dominant mechanism for bulk phase transitions. In small volumes, it is statistically unlikely that each compartment will have a heterogeneous site; thus, nucleation occurs by homogeneous initiation. Homogeneous nucleation mechanisms for HD in mini-emulsions were reported

dx.doi.org/10.1021/jp211459j | J. Phys. Chem. B 2012, 116, 3954−3960

by Montenegro et al., but they did not see a significant variation of particle size at the freezing point of the oil.[21] We have previously reported on the freezing point for HD encapsulated within poly(alkyl- methacrylate) capsules, where the alkyl backbone was varied between methyl, ethyl, *n*-butyl, *t*-butyl, and *n*-hexyl groups. This was done to vary the surface tension of the oil/polymer interface. In our previous work, we noted a slight change in the freezing point with size that seemed to agree with Gibbs–Thomson-like behavior for poly(methyl methacrylate capsules).[33]

For this study, a series of PtBMA capsules containing pure HD were synthesized. The volume of the encapsulated HD was varied using both sonication time (constant monomer/HD ratio) and the monomer/HD ratio (90 s sonication time). The particles in the study vary both in overall size and polymer thickness, but the oil droplet volume was calculated from eq 1 above. Figure 8 shows the freezing point of the encapsulated

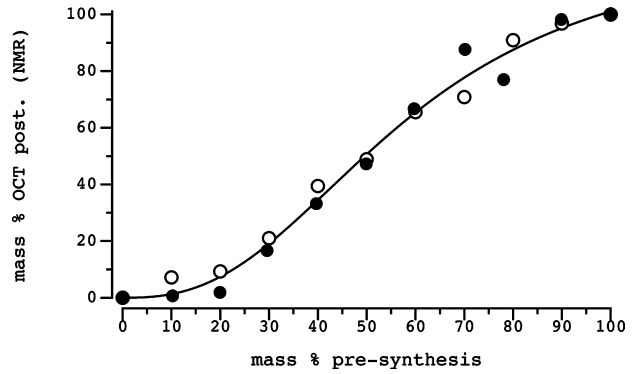

Figure 7. The measured mass fraction of OCT in the capsule as a function of the mass fraction of OCT used in the synthesis.

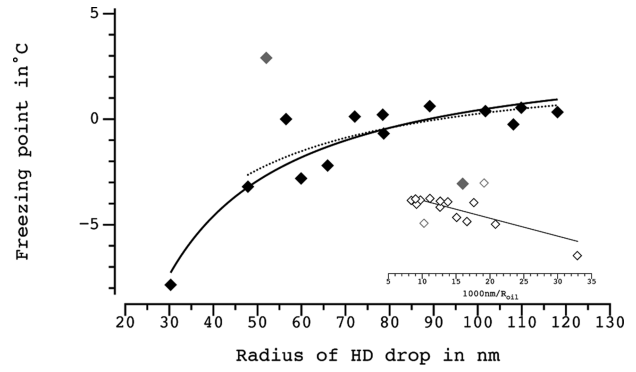

Figure 8. Freezing point of encapsulated HD as a function of the calculated oil droplet size. The inserted figure plots the freezing point as a function of inverse radius of the oil droplet. Points ignored from the fit are included in gray.

HD as a function of the calculated radius of the oil droplets. The regression line through the points follows the trend expected from the Gibbs–Thompson equation:

$$T_{f,drop} = T_{f,bulk} - \frac{K}{R_l} \quad (3)$$

with

$$K = \frac{4T_{f,bulk}\gamma_{s/l}}{\Delta H_f \rho_l}$$

where $\gamma_{s/l}$ is the interfacial tension between the liquid phase and the adjacent solid phase (polymer), ΔH_f is the enthalpy of freezing for the liquid phase, ρ is the density of the liquid phase, and R is the radius of the droplet.

The fit through the data follows the equation T_f (°C) = 3.77 − 335/R (nm) with some obvious outliers. The data point from the smallest oil droplet has a large effect on the fitted line, but omitting this point (dashed line on graph) lessens the confidence of the fit (both R^2 and σ for the residuals). It is important to note at this point that the limit of infinite radius does not approximate the bulk freezing point of HD (18 °C). Furthermore, we note that if the oil droplet radius ranges around 100 nm, a small variation in droplet volume does not have a marked effect on the freezing point of the oil phase. This behavior agrees with our previous work, but here we have more experimental values for the PtBMA system. We focus our subsequent work on particles with an oil radius of approximately 90 ± 10 nm.

Phase Transition Temperatures of Bulk and Encapsulated *n*-Hexadecane/1-Octanol Solutions. Figure 9 shows

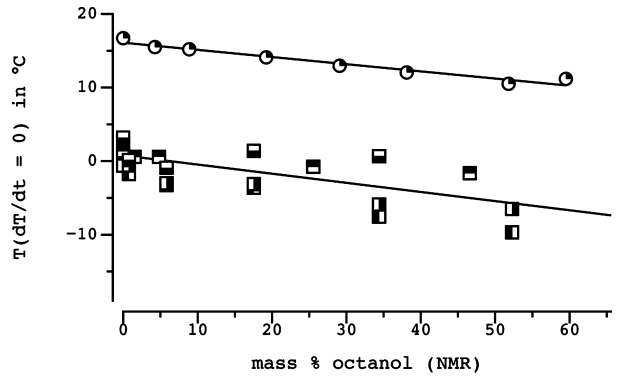

Figure 9. Onset temperatures for freezing of HD/OCT solutions in bulk and in capsule dispersions. Circles represent measured bulk values, whereas squares represent the measured freezing point in encapsulated solutions.

the freezing points of HD in bulk and in PtBMA capsules as a function of the mass % of OCT in the oil (NMR).

Capsules with an OCT fraction greater than 60% showed multiple transitions in the DSC thermograms, and the phase transition temperature was very close to the freezing point of the water in the sample. This made the determination of onset temperature unreliable and the determination of transition enthalpy impossible. Furthermore, the peak for the HD phase transition in the bulk samples was also affected by the transition of the OCT in the sample at OCT fractions higher than 60%.

The freezing and melting point of bulk HD decreased with increasing OCT fraction. We expect this property in the bulk phase. The reduction appears to be linearly correlated with the mass fraction of OCT, x_m, or $T_{f,HD}(x_m) = 17.2 - 0.10 \cdot x_m$. The freezing point of HD in the capsules was significantly lower than that in the bulk phase. This agrees with previously reported anomalous freezing behaviors of encapsulated HD.

In addition to seeing an approximate difference of 16 °C, or K, between the freezing points in bulk and capsules, our measurements show that the freezing point of the encapsulated HD has a nearly identical dependence on the mass fraction of OCT, $T_{f,HD}(x) = 0.78 - 0.12 \cdot x$. The freezing point depression

dx.doi.org/10.1021/jp211459j | J. Phys. Chem. B 2012, 116, 3954–3960

due to the OCT is therefore the same in the bulk as it is in the encapsulated volume.

In bulk HD, the freezing point and melting point are not identical, even in the limit of infinitely slow cooling. Taggart et al.[28] demonstrated this in several pure hydrocarbon oils, and dubbed the difference the metastable zone width, or mszw = $\lim_{dT/dt\to 0}(T_m - T_f)$. According to Taggart, mszw varies with the type of crystal structure formed when the oils freeze. In particular, pure HD has a metastable zone width of approximately 2.3 °C (or K) as the oil crystallizes in a triclinic structure. Figure 10 shows the measured mszw for the samples

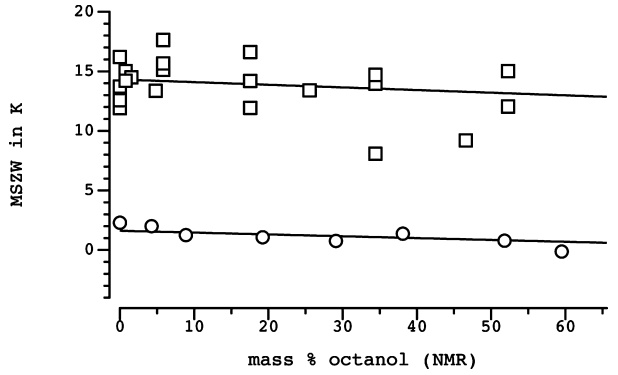

Figure 10. Metastable zone width for encapsulated HD (squares) and bulk HD (circles) as a function of the mass fraction of OCT in the binary phase.

shown in Figure 9. Linear fits are included in the figure to guide the eye, yielding the equations mszw(x) = 1.6 − 0.015·x for the bulk phase and mszw(x) = 14.3 − 0.022·x for the encapsulated phase. Here x is the mass fraction of OCT in the sample as determined by NMR. The value we obtained for bulk HD closely agrees with the published values of Taggart et al.

The mszw in the bulk decreases noticeably with increased fraction of OCT in the solution. This is a behavior we would expect, since OCT is likely to disrupt the triclinic packing of HD in the bulk. We see a very similar decrease in the mszw for encapsulated HD, while the absolute value of the mszw remains very large.

Phase Transition Enthalpies of Bulk and Encapsulated *n*-Hexadecane/1-Octanol Solutions. Figure 11 shows the

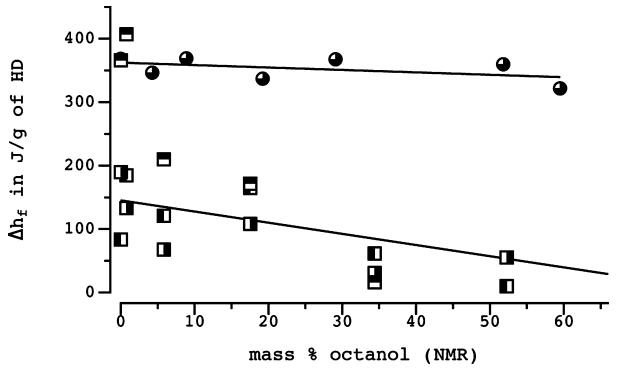

Figure 11. Specific enthalpies of freezing for bulk (circles) and encapsulated (squares) HD in binary mixtures of OCT and HD at various mass fractions of OCT.

values for the specific enthalpy of freezing per gram of HD, $\Delta h_{s,f}$(HD), as a function of the composition of the binary solution. $\Delta h_{s,f}$(HD) was calculated by measuring the area under the DSC thermogram. The area was then multiplied by the heating rate and divided by the calculated mass of HD in the solution. Similar values were calculated for OCT in the solution, but these data are not shown in the figure. HD in the bulk samples was weighed directly on a microbalance, but the mass of HD in the capsules had to be calculated from quantitative NMR measurements as described above. Similar quantitative NMR measurements yielded mass for the bulk samples within 5% of the weighed values. The mass calculated for the encapsulated samples is prone to error due to two factors: (1) The signal relaxation time for the encapsulated volumes is faster than the signal relaxation for the bulk samples (in chloroform). This causes the mass to be underestimated in the sample. (2) The capsules float to the top of the sample tube when allowed to rest for a long time. Although the flotation of the sample is macroscopically slow, we noticed a slight reduction in signal intensity if the samples were left in the spectrometer for longer periods of time.

Our measured value for $\Delta h_{s,f}$(HD) in the pure, bulk HD agrees well with values found in the literature. We saw little variation in $\Delta h_{s,f}$(HD) as we increased the fraction of OCT in the bulk system, which indicates that HD and OCT form solutions that have a nearly ideal mixing behavior. Linear fit through the data gave $\Delta h_{s,f}$(HD) = 362 − 0.38·x_m(OCT).

The encapsulated HD showed a very different absolute value for Δh_s than the bulk with the exception of two experimental trials. Additionally, x_m of OCT appears to affect Δh_s in the capsules more strongly than in the bulk. Linear fits through the data gave $\Delta h_{s,f}$(HD) = 145 − 1.8·x_m(OCT). It should also be noted that, at higher fractions of octanol, $\Delta h_{s,f}$(HD) seemed to plateau out at 50 ± 10 J/g.

The information gathered for enthalpy in Figures 9 and 11 can be combined to calculate the specific entropy of the phase transition when the hexadecane freezes. The data points are quite scattered, but the linear fit through the data given in the text can be used to get an estimate of the entropy exchanged in the transformation. Doing this reveals that the change in entropy in the confined phase is greatly reduced from the bulk value and is more affected by the change in composition of the oil phase in the capsule.

SUMMARY AND DISCUSSION

The synthesis of PtBMA capsules containing a high volume fraction of binary oil solution consisting of 1-octanol and *n*-hexadecane was successful. Capsules with binary mass compositions ranging from 0% OCT to 80% OCT were prepared with good yields. Capsules with higher OCT fractions had substantially lower yields.

In studying the capsules, we found that the mass fraction of OCT in the synthesis was not always the same as the mass fraction in the harvested capsules. Synthetic formulations with low OCT fraction showed lower final composition of the alcohol, whereas formulations with high OCT fractions resulted in capsules with even higher OCT fractions.

The sigmoidal shape of Figure 7 is similar to cooperative binding isotherms. If there is a cooperative effect contributing to the solubility of oils in microvolumes due to surface wetting and surface packing, the oil droplets may restrict a minority component to smaller droplets in the system. Smaller droplets have a lower probability of containing sufficient amounts of monomer and initiator to result in stable capsules after

dx.doi.org/10.1021/jp211459j | J. Phys. Chem. B 2012, 116, 3954−3960

polymerization. The smaller droplets are therefore removed during the purification process.

In Figure 8, we observe a clear effect of oil droplet size on the freezing point in the HD. This behavior is in agreement with the Gibbs−Thomson equation with one significant exception; Gibbs−Thomson predicts that the freezing point will asymptotically approach the bulk phase transition temperature in the limit of infinite particle size. This is clearly not the case in Figure 8, unless the solid HD that forms in the capsules has a different crystal structure than formed from the bulk HD. This is something we may in fact expect, since a large fraction of the HD is very close (less than five monolayers) to the polymer layer.

A different crystal structure could also be the underlying reason for the difference in transition enthalpy that we observe between capsules and bulk in Figure 11. The difference in the absolute enthalpy values between bulk and capsules is beyond what we would consider reasonable experimental error, even when considering errors in the NMR quantitation due to differences in signal relaxation rate between bulk phases and encapsulated volumes. An alternative explanation for this could be that only a small fraction of HD freezes in the presence of OCT in the encapsulated system. So far, our variable temperature NMR experiments have shown that the majority of HD is solid in the capsules once the sample reaches the onset temperature that we measure in the DSC runs. Our preliminary data indicate that there is a slight variation in the fraction of HD that becomes solid with particle size and the type of polymer used to encapsulate the droplet, but the fraction that remains liquid is quite small in all instances.

The large metastable zone width, mszw, that we see in Figure 10 can also be accounted for if we assume that the encapsulated oil phase forms a crystal structure upon freezing that is different from the bulk oil. Our observed mszw of 14 °C is far greater than the 2.3 °C difference that Taggart reported for pure bulk HD. In their work, scattering experiments showed triclinic crystal structure in the bulk, whereas here we would expect a highly disordered structure due to the curvature of the interface, thus a greater metastable zone.

■ ASSOCIATED CONTENT

Supporting Information

A tabulated summary of the measured values for the freezing and melting point of HD and OCT as well as the measured specific enthalpies for the phase transitions for the bulk systems are collected in Table 1 in the supplemental information for this paper. A tabulated summary of the freezing point and the enthalpy of freezing for the encapsulated HD/OCT systems can be found in Table 2 in the supplemental information. This material is available free of charge via the Internet at http://pubs.acs.org.

■ AUTHOR INFORMATION

Corresponding Author

*E-mail: tadalsteinsson@scu.edu.

Notes

The authors declare no competing financial interest.

■ ACKNOWLEDGMENTS

The authors thank the UCSC-MACS Facility at Ames Research Center for generous funding for training on TEM instrumentation as well as access to this instrument. Funding for this project was provided by Santa Clara University Faculty Development Program as well as the Department of Chemistry & Biochemistry at SCU. The acquisition of the NMR spectrometer by SCU was through NSF-MRI Grant #0923575.

■ REFERENCES

(1) Tiarks, F.; Landfester, K.; Antonietti, M. *Langmuir* **2001**, *17*, 908−918.
(2) Soto-Portas, M. L.; Argillier, J. F.; Mechin, F.; Zydowicz, N. *Polym. Int.* **2003**, *52*, 522−527.
(3) Dowding, P. J.; Atkin, R.; Vincent, B.; Bouillot, P. *Langmuir* **2004**, *20*, 11374−11379.
(4) Jiang, B. B.; Gao, C. Y.; Shen, J. C. *Colloid Polym. Sci.* **2006**, *284*, 513−519.
(5) Jagielski, N.; Sharma, S.; Hombach, V.; Mailander, V.; Rasche, V.; Landfester, K. *Macromol. Chem. Phys.* **2007**, *208*, 2229−2241.
(6) van den Dungen, E. T. A.; Klumperman, B. *J. Polym. Sci., Part A: Polym. Chem.* **2010**, *48*, 5215−5230.
(7) Bernardy, N.; Romio, A. P.; Barcelos, E. I.; Pizzol, C. D.; Dora, C. L.; Lemos-Senna, E.; Araujo, P. H. H. *J. Biomed. Nanotechnol.* **2010**, *6*, 181−186.
(8) Siquing, C.; Guo, Y.; Zetterlund, P. B. *Macromolecules* **2010**, *43*, 7905−7907.
(9) Velikov, K. P.; Pelan, E. *Soft Matter* **2008**, *4*, 1964−1980.
(10) DeMaggio, G. B.; Frieze, W. E.; Gidley, D. W.; Zhu, M.; Hristov, H. A.; Yee, A. F. *Phys. Rev. Lett.* **1997**, *78*, 1524−1527.
(11) Reiter, G. *Phys. Rev. Lett.* **1992**, *68*, 75−78.
(12) Tsui, O. K. C.; Russell, T. P.; Hawker, C. J. *Macromolecules* **2001**, *34*, 5535−5539.
(13) Israelachvili, J. N. *J. Colloid Interface Sci.* **1996**, *110*, 263−271.
(14) Lum, K.; Chandler, D.; Weeks, J. D. *J. Phys. Chem. B* **1999**, *103*, 4570−4577.
(15) Senapati, S.; Chandra, A. *J. Phys. Chem. B* **2001**, *105*, 5106−5109.
(16) Raviv, U.; Laurat, P.; Klein, J. *Nature* **2001**, *413*, 51−54.
(17) Turnbull, D. *J. Chem. Phys.* **1952**, *20*, 411−424.
(18) Turnbull, D.; Cormia, R. L. *J. Chem. Phys.* **1961**, *34*, 820−831.
(19) Kozisek, Z.; Demo, P. *J. Aerosol Sci.* **2009**, *40*, 44−54.
(20) Kozisek, Z.; Demo, P. *J. Aerosol Sci.* **2009**, *40*, 802−806.
(21) Montenegro, R.; Antonietti, M.; Mastai, Y.; Landfester, K. *J. Phys. Chem. B* **2003**, *107*, 5088−5094.
(22) Jiang, K.; Su, Y. L.; Xie, B. Q.; Jiang, S. C.; Zhao, Y.; Wang, D. J. *J. Phys. Chem. B* **2008**, *112*, 16485−16489.
(23) Menahem, T.; Mastai, Y. *New J. Chem.* **2008**, *32*, 925−928.
(24) Kai, J.; Baoquan, X.; Shichun, J.; Ying, Z.; Dujin, W. *J. Phys. Chem. B* **2008**, *112*, 16485−16489.
(25) Dongsheng, F.; Yulan, S.; Baoquan, X.; Haijin, Z.; Guoming, L.; Dujin, W. *Phys. Chem. Chem. Phys.* **2011**, *13*, 2021−2026.
(26) Gelb, L. D.; Gubbins, K. E.; Radhakrishnan, R.; Sliwinska-Bartkowiak, M. *Rep. Prog. Phys.* **1999**, *62*, 1573−1659.
(27) Wu, X. Z.; Sirota, E. B.; Sinha, S. K.; Ocko, B. M.; Deutsch, M. *Phys. Rev. Lett.* **1993**, *70*, 958−961.
(28) Taggart, A. M.; Voogt, F.; Clydesdale, G.; Roberts, K. J. *Langmuir* **1996**, *12*, 5722−5728.
(29) Madariaga, J. A.; Santamaria, C.; Bou-Ali, M. M.; Urteaga, P.; Mezquia, D. A. D. *J. Phys. Chem. B* **2010**, *114*, 6937−6942.
(30) Hindle, S.; Povey, M. J. W.; Smith, K. *J. Colloid Interface Sci.* **2000**, *232*, 370−380.
(31) Kai, J.; Baoquan, X.; Yanfeng, M.; Dujin, W. *J. Phys. Chem. B* **2009**, *113*, 3269−3272.
(32) Fette, E. V.; Pham, A.; Adalsteinsson, T. *J. Phys. Chem. B* **2008**, *17*, 5403−5411.
(33) Black, J. K.; Tracy, L. E.; Roche, C. P.; Henry, P. J.; Pesavento, B.; Adalsteinsson, T. *J. Phys. Chem. B* **2010**, *114*, 4130−4137.
(34) Landfester, K.; Bechthold, N.; Tiarks, F.; Antonietti, M. *Macromolecules* **1999**, *32*, 5222−5228.
(35) Charoenrein, S.; Reid, D. S. *Thermochim. Acta* **1989**, *156*, 373−381.